Study of vessel shape effect on charge/discharge rates of a silicon-based LHTES system

Zeneli M. [a, b], Nikolopoulos A. [a], Nikolopoulos N. [a], Karellas S. [b], Kakaras E. [a, b]

[a] *Centre for Research and Technology Hellas, Chemical Process & Energy Resources Institute (CERTH/CPERI). Athens, Greece, zeneli@certh.gr*
[b] *Laboratory of Steam Boilers and Thermal Plants National Technical University of Athens 9, Zografou, Greece*

Abstract:

This work presents a validated computational fluid dynamics (CFD) model able to simulate the solidification/melting process of high energy density phase-change materials (PCM), such as silicon. Storage devices utilizing such PCMs can be used in power-to-heat-to-power (P2H2P) systems, to store heat in high temperature and use it for electricity production. Prior to manufacturing such a device, there is a necessity to scrutinize the complex heat transfer mechanisms occurring during the phase change of the contained PCM and indicate a flexible vessel design that enables quick charge/discharge rates and low heat losses during storage period. The CFD model, which is developed in Fluent v17.0 platform, combines the volume of fluid method with the enthalpy porosity approach and an adaptive local grid refinement method, able to achieve a sharp gas/PCM and solid/liquid PCM interface. In contrast to analytical or other CFD models available in the literature, this one takes into account the PCM volume change during solidification/melting, possible dendrites formation and buoyancy-driven natural convection effect on heat transfer mechanisms. Numerical results unveil that the system charge/discharge rates are highly dependent on the PCM permeability and vessel design. Between five shapes investigated, i.e. cylinder, cube, truncated cone, sphere and cut-off sphere, of volume V_{vessel}=3.75E-03 m^3, the truncated cone is the most suitable solution for a P2H2P application, considering design flexibility, melting rates and heat losses. Actually, the PCM melting time achieved with the cone is 21% quicker compared to sphere and only 6% slower compared to cube; the latter is the optimum geometry, as concerns charge rates, but it should be avoided because of its excess lateral losses during storage period. During discharging, when heat is extracted from the vessel bottom, the truncated cone results in the lowest solidification rates, almost 50% lower than the cut-off sphere, which is the optimum shape in terms of discharge rates. Nevertheless, the truncated-cone discharge rates can be further improved by altering its height, without increasing its volume. In practice, the current model is of high accuracy and can give optimization guidelines for the design of such and similar LHTES systems.

Keywords:

Computational fluid dynamics (CFD), Silicon solidification/melting, Vessel shape investigation, Volume of fluid method.

1. Introduction

During the forthcoming years, the employment of thermal energy storage systems (TES) will boost the energy transition from fossil fuels to renewable energy sources, such as solar energy. In this context, latent heat thermal energy storage (LHTES) systems that use phase change materials (PCM) to store thermal energy offer the ability to unlock energy densities greater than the ones achieved with sensible systems and on a nearly constant temperature range. Up until recently, PCMs of low thermal conductivities –usually molten-salts- have been used, resulting in low system charge/discharge rates [1]. Storage at ultra-high temperatures (>900 ºC) with the utilization of metallic PCMs characterized by high thermal conductivities and heat of fusion, such as Si, B and/or their alloys, can increase even further those systems energy density -more than 20-times higher than conventional molten-salt based systems [2]. Hence, the storage efficiency of such systems is highly dependent on the PCM thermal properties, including thermal conductivity, specific heat, latent heat of fusion and melting point. Other crucial factors affecting those systems thermal performance are the PCM container design and operating conditions [3]. Therefore, studying in detail the transient heat transfer mechanisms of LHTES systems during charge/discharge phase, and quantification of key parameters, such as solidification/ melting rates, power outputs and heat losses is a necessity to achieve their optimization.

Notwithstanding, the energy performance of LHTES systems is a complicated issue to assess. The main reason is that during the PCM phase change occur phenomena that significantly affect the heat transfer process, including a) buoyancy-driven natural convection, b) PCM expansion/contraction, and c) dendrites formation in the solid PCM [4]. During the last decades, many analytical and numerical studies have focused on the thermal performance of various PCMs, inside spherical, cylindrical and rectangular containers [5]. Moore et al. [6] set the grounds of the ''unconstrained'' melting method, i.e. the prediction of the solid floating (sinking) in the molten PCM and the subsequent PCM volume increase. Later on, Limburg et al. [7] studied numerically the solidification/melting process of paraffin at low temperatures using the unconstrained enthalpy-porosity approach [8]. They proved that when natural convection is neglected from the model, a high error is induced in the numerical results. Nevertheless, the majority of the published numerical studies neglect the aforementioned phenomena and their effect on the solidification/melting process [9], [10].

Furthermore, very few reports are focusing on PCMs with phase change temperature exceeding 100 ºC. Archibold et al. [11] in their work analyzed the solidification/melting process of $NaNO_3$ as a PCM, at 306.8 ºC, inside a spherical container. Elmozughi et al. [12] used the enthalpy-porosity approach coupled with the VOF model to simulate the $NaNO_3$ melting inside spherical and cylindrical shells up to 500 ºC. Pirasaci et al. [13] worked on the same temperature range (~500 ºC) to study the melting process of an encapsulated Na_2SO_4 – KCl eutectic mixture. Finally, Veeraragavan et al. [10] studied the pure Si solidification process at ultra-high temperature (~1400 ºC), by neglecting, however, the PCM volume change. Arising from this research is the need to form an efficient and accurate numerical model that will study high temperature (>1000 ºC) latent heat thermal energy storage processes, by simultaneously taking into account the complex heat transfer mechanisms and the PCM structure and system geometric parameters effect on the heat transfer process.

In this work, an advanced transient computational fluid dynamics (CFD) model that describes the complex heat transfer mechanisms occurring during the charge and discharge phase of LHTES systems is presented. This model integrates the volume of fluid method with the enthalpy porosity approach and takes into account, a) the PCM volume change, b) buoyancy driven natural convection c) PCM thermal properties and permeability and d) vessel design effect on the heat transfer process. In order to enhance its efficiency and accuracy, an adaptive local grid refinement method is utilized. Initially, the model is validated against experimental data and numerical results retrieved from Assis et al. [14], [15], for the solidification/melting of paraffin wax at temperatures near 30ºC. Later on, the thermal performance of a Si-based LHTES system operating at ultra-high temperatures is numerically studied using different designs, during charge (melting) and discharge (solidification) process, under no heat losses conditions. Five different container designs are studied, i.e. sphere, cut-off sphere, truncated-cone, cylinder and cube. Supplementary indicative values of the system heat losses during

storage period are calculated. The parametric study is conducted to optimize the design and to evaluate the system thermal performance. The key parameters considered in this analysis are the charge/discharge rates during the system thermal cycling and heat losses during storage period. To the best of our knowledge, for the first time, such an accurate and efficient CFD model is implemented for the simulation and design optimization of a LHTES operating at ultra-high temperatures.

2. Numerical methodology

The CFD model presented in this work is implemented in ANSYS Fluent platform (v17.1) [16] to simulate the solidification/melting process of silicon inside a sealed gas-PCM vessel. This model is based on the enthalpy-porosity approach [8] coupled with the volume of fluid (VOF) model. It is accompanied by the inclusion of compressibility effects of the contained gas, which can be either compressed inside the sealed shell, due to PCM expansion, or exit the container through a release valve or a small opening. For a more accurate treatment of the gas-PCM and solid-liquid interfaces, an adaptive local grid refinement [17] method is applied, by means of several user-defined functions (UDFs); this method enhances the numerical results accuracy without substantially increase of the computational cost. It should be noted that the current model has been previously verified against an analytical model [18], describing the silicon solidification process inside a sealed crucible at ultra-high temperatures. However, in order to enhance its validity, it is compared against experimental data retrieved from the literature, for the paraffin wax solidification/ melting case at low temperatures.

The conservation equations of mass (1), momentum (2), and energy (3) used in this model are:

$$\frac{\partial a_n}{\partial t} + \frac{\partial a_n u_i}{\partial x_i} = 0 \tag{1}$$

$$\frac{\partial}{\partial t}(\rho u_i) + \frac{\partial}{\partial x_j}(\rho u_j u_i) = -\frac{\partial p}{\partial x_i} + \mu \frac{\partial^2 u_i}{\partial x_j x_j} + \rho g_i + S_i \tag{2}$$

$$\frac{\partial}{\partial t}\rho H + \frac{\partial}{\partial x_i}(\rho u_i H) = \frac{\partial}{\partial x_i}\left(k \frac{\partial T}{\partial x_i}\right) + S \tag{3}$$

In equation (3), S is a source term due to volumetric energy generation, viscous dissipation, etc., and H is the specific enthalpy, which is the sum of the sensible enthalpy (h) and the latent heat (ΔH):

$$H = h + \Delta H \tag{4}$$

$$h = h_{ref} + \int_{T_{ref}}^{T} c_p dT \tag{5}$$

, where h_{ref} is the enthalpy at the reference temperature ($T_{ref} = 25\ ^{\circ}C$).

The latent heat is calculated according to the following equation:

$$\Delta H = \beta L \tag{6}$$

, where β is the liquid fraction defined as:

$$
\begin{aligned}
\beta &= 0 & &\text{if } T < T_{solidus} \\
\beta &= \frac{T - T_{solidus}}{T_{liquidus} - T_{solidus}} & &\text{if } T_{solidus} < T < T_{liquidus} \\
\beta &= 1 & &\text{if } T > T_{liquidus}
\end{aligned}
\tag{7}
$$

, and the indexes solidus and liquidus denote the PCM solid and liquid phases, respectively.

Hence, the latent heat varies from zero to L, depending on the local temperature T at each computational cell. An artificial region, called mushy zone, is assigned to encounter the phase change within a finite temperature range between the PCM solid and liquid phases, i.e. $T_{solidus} < T < T_{liquidus}$. This region is actually formed in metal alloys (e.g. Si/B mixture) or paraffins during their phase change, but not in pure metals, such as Si. Nonetheless, this assumption is necessary from a numerical point of view to achieve a smooth transition of the PCM properties around its melting point.

The term S_i used in equation (eq. 2) is the momentum dissipation source term and is equal to:

$$S_i = -A_{mush} \frac{(1-\beta)^2}{\beta^3 + \varepsilon} u_i \qquad (8)$$

, where ε is equal to 0.001 and is used to avoid a possible zero denominator (when $\beta = 0$). A_{mush} is the mushy zone parameter, and is dependent on the dendrites formed during solidification process, the material density (ρ) and viscosity (μ), parameters that reflect the PCM permeability [19]:

$$A_{mush} = 180 \frac{\mu}{\rho DAS^2} \qquad (9)$$

, where DAS is the secondary dendrites arm spacing.

The model has the following characteristics and assumptions:

1. Transient fluid flow and heat transfer mechanisms is considered;
2. Solution of an axisymmetric problem, for the geometries that are symmetric to an axis, i.e. sphere, cut-off sphere, cone and cylinder. In the case of a cubic vessel a 3D problem is solved;
3. Inclusion of gravity and buoyancy-driven natural convection effect;
4. The flow is considered laminar, due to low Reynolds numbers for all the cases studied;
5. The molten PCM is treated as an incompressible Newtonian fluid;
6. The PCM solid and liquid phases are homogeneous and isotropic;
7. The PCM thermophysical properties are dependent on temperature variations;
8. The PCM viscosity in the cells, where the liquid fraction is equal to zero, is set to a high value, i.e. equal to 10 kg·m^{-1}·s^{-1}, so that the solver can virtually understand that in the particular cell the material behaves as solid. This approach is similar to the one followed in the work of [20];
9. The inert gas is treated as a compressible fluid, by solving Tait equation [16], if the container is sealed (silicon case) and as incompressible, if the container is open (paraffin wax case);
10. Radiative heat transfer within the PCM is neglected;
11. Adiabatic conditions are assumed during PCM solidification/ melting phase;
12. Contact thermal resistance between PCM and walls is considered negligible;
13. The crucible walls are modelled as thin walls, by solving a 1D heat conduction equation;

Finally, for the VOF formulation, an implicit scheme is used, with a sharp interface modelling type, whilst the interfacial anti-diffusion treatment algorithm is enabled to eliminate numerical diffusion.

3. Numerical cases examined

3.1. CFD model validation

Initially, the CFD model is validated against experimental data for the solidification/ melting process of paraffin wax, RT27, at low temperatures, i.e. ~30 ºC, inside a spherical casing open from the top. Such data along with the appropriate boundary and operating conditions are obtained from the work of Assis et al. [14], [15]. During melting (solidification) process, the vessel is heated (cooled) from its walls, almost 10 ºC above (20 ºC below) its melting point, Figure 1a. The applied grid methodology follows the local grid refinement method with two refinement levels, Figure 1b. This results in a maximum number of quadrilateral cells equal to 11,133 and a minimum cell size equal to 1.07·10^{-4} m.

During model validation, a parametric study is conducted as concerns the A_{mush} parameter effect on the PCM solidification/ melting rate. A set of A_{mush} values equal to [10^5, 5·10^5 and 2·10^6] and [10^5, 10^6 and 10^9] are tested during melting and solidification phase, respectively.
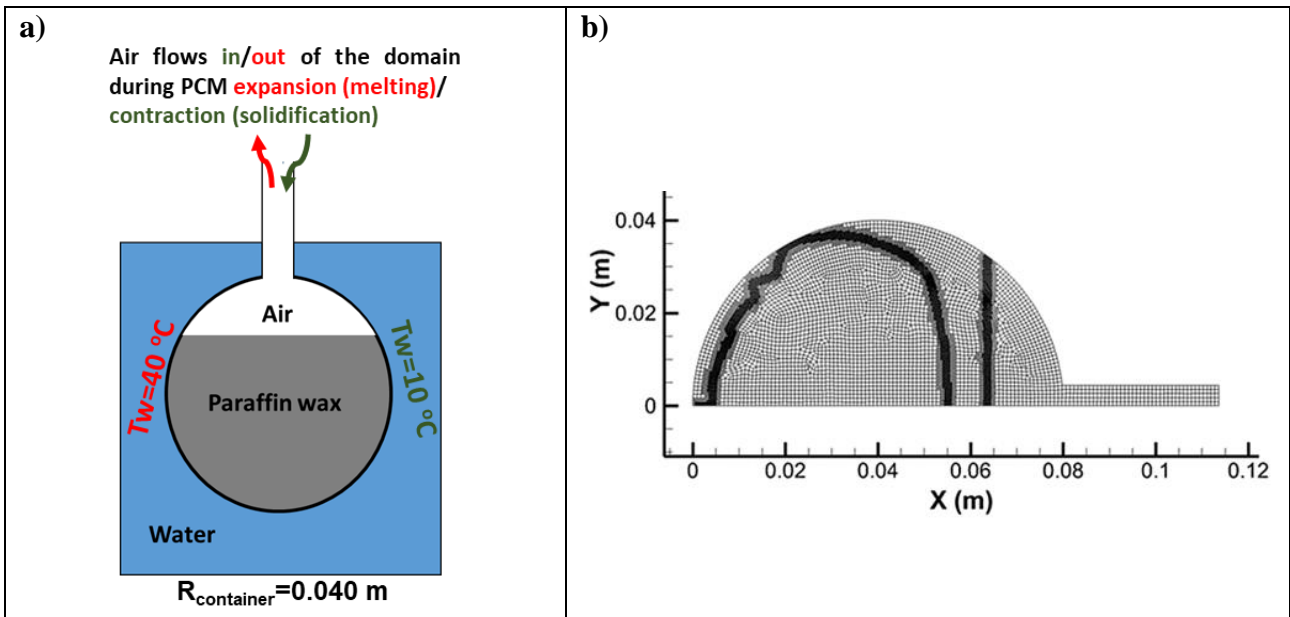
Figure 1. a) Two-dimensional (2D) scheme of the PCM container and b) discretized domain constructed with the adaptive local grid refinement technique (2 Levels of refinement).

3.2. Vessel shape/ size parametric investigation

3.2.1. Geometry and Mesh layout

Following its validation the CFD model is applied for the numerical study of Si solidification/ melting process at ultra-high temperatures (~1400 ℃) inside a novel electric-TES system, described in [2]. Five different TES design concepts are studied (Figure 2), i.e. sphere, cut-off sphere, cylinder, truncated cone and cube, with the same volume (V_{vessel} = 3.75E-03 m^3) and emitter surface (A_{Em}=2.25E-02 m^2)–vessel bottom area where the heat extraction occurs during discharging. All the tested geometries are created in ANSYS DesignModeller and they are sealed from the top.
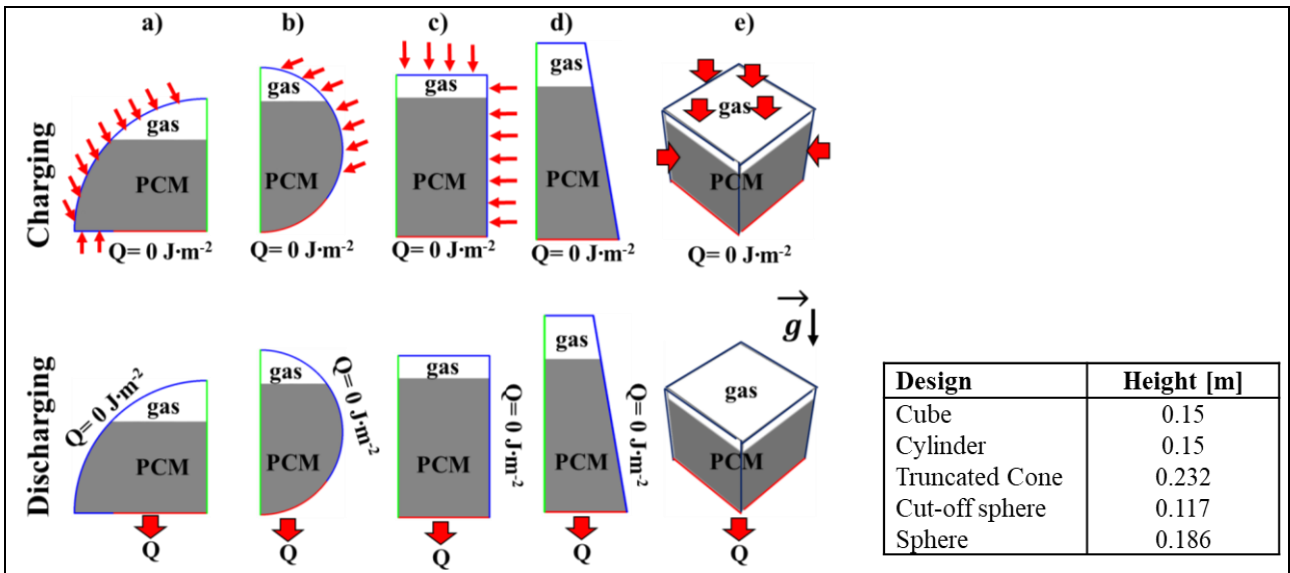

Figure 2. Physical models of the studied geometries: (a) cut-off sphere, (b) sphere, (c) cylinder, (d) truncated cone and (e) cube. Red: emitter, green: axis, Blue: sidewalls.

The applied grid methodology follows the local grid refinement method with two refinement levels, as in the model validation. Table 1 provides information on the number of cells required to achieve the sharp gas-PCM and solid (PCM)–liquid (PCM) interface by using either the local grid refinement technique or an equivalent uniform dense grid of the same grid resolution near the interfaces. It can

be inferred that implementation of the local refinement can notably decrease the number of cells necessary to achieve the desirable interface and as a consequence speed-up the computational process.

Table 1. Mesh details for the different geometries tested.

Design	Grid	# Cells	# Cells of equivalent dense grid	Problem
Cube	2 Lev. ref.	~7.5·105	~3·106	3D
Cylinder	2 Lev. ref.	~1.6·104	~7·104	Axisymmetric
Cone	2 Lev. ref.	~1.1·104	~4·104	Axisymmetric
Cut-off sphere	2 Lev. ref.	~1·104	~4.9·104	Axisymmetric
Sphere	2 Lev. ref.	~1.1·104	~5.9·104	Axisymmetric

3.2.2. Boundary, Operating and Initial conditions

The problem boundary conditions imposed on the five tested geometries during Si melting are presented in Table 2. More specifically, the container sidewalls are heated at a uniform temperature equal to 1707 °C. The emitter is insulated during melting, as the device is in "charging" mode, thus, no heat loss conditions are considered there. Additionally, the contact resistance R_c is set equal to zero, following the assumption that there is not an additional air gap between the walls and the PCM and a no slip boundary condition is set at the solid boundaries, as in the work of Assis et al. [14]. The wall thermal resistance, R_w, is considered equal to the one used in the model validation case. However, in ultra-high temperature LHTES systems, crucibles of lower R_w (such as ceramic materials) are used.

Initially, the PCM occupies the 92% of the domain, which is subcooled with a temperature 10 degrees lower than the PCM melting point, i.e. 1413 °C.

Table 2. Boundary conditions imposed during the study of vessel shape effect on Si melting.

	BC type	Parameters	Units	Values
Sidewalls	Wall	T_W	°C	1707
		R_W	m² K W⁻¹	0.0025
		R_c	m² K W⁻¹	0
Emitter	Wall	Q_{Em}	W m⁻²	0
	Shear condition at walls: No slip			
Axis	Symmetry			

The PCM solidification process is simulated shortly after its melting phase. In this case, heat is extracted from the vessel bottom part, making the dominant heat transfer direction the vessel axis. A uniform temperature is set at this surface equal to 1097 °C, whilst zero heat losses are considered at the sidewalls, Table 3. Initially, the molten PCM fills 86.2% of the domain, due to its contraction after melting. Additionally, the whole domain is patched with temperature 5 degrees greater than the PCM melting point.

Table 3. Boundary conditions imposed during the study of vessel shape effect on Si solidification.

	BC type	Parameters	Units	Values
Emitter	Wall	T_W	°C	1097
		R_W	m² K W⁻¹	0.0025
		R_c	m² K W⁻¹	0
Sidewalls	Wall	Q_W	W m⁻²	0
	Shear condition at walls: No slip			
Axis	Symmetry			

In both phases, transient calculations are performed, with a variable time step size (courant number =0.2). Information on the discretization schemes and the gas-silicon properties can be found in [18].

4. Results

4.1. CFD model validation

Figure 3a compares the melting fraction results as a function of time of the applied CFD model with the ones obtained from Assis et al. [14], both numerical model and experiments. The model applied by Assis, utilizes a grid of 3,520 cells– in contrast to the current model that uses the adaptive local grid refinement method. The melting fraction parameter used for comparison is calculated as the ratio between the liquid PCM mass over the total PCM mass ($MFR= m_{liquid}/m_{PCM}$), at a given moment. From the graph, it is proven that for most of the simulation time, the numerical results of the CFD model virtually coincide with that of the reference paper and are close enough to the experimental data. The small deviation, almost equal to 6 %, between the two models, can be primarily attributed to the different meshing methods used –coarse fixed grid in the reference paper and an adaptive local grid refinement method in the current model. Furthermore, in the reference paper, there are not any details available concerning the spatial and time discretization schemes and VOF formulation (implicit or explicit), the selection of which can affect the numerical results.

In the same graph, quantitate results of the A_{mush} parameter versus time are depicted. It can be deduced that this parameter affects significantly the PCM melting rate. An A_{mush} value equal to $5 \cdot 10^5$, which corresponds to a dendrites arm spacing equal to DAS=0.4 μm, gives the most accurate results for the melting performance of the specific PCM studied, i.e. paraffin wax. Thus, the values of this parameter should not be chosen arbitrarily, since A_{mush} is dependent on the solid PCM morphology, which in turn is highly affected by the imposed cooling rate [21]. Numerically, the dendrites presence in the solid PCM and subsequently the PCM permeability are modelled implicitly. Decrease in the A_{mush} parameter, which considers higher DAS values and, subsequently, higher permeability, increases the velocity values in the mushy zone, allowing significant flow motion in that region. This in turn accelerates the heat transfer, through convection, at the vicinity of that area.
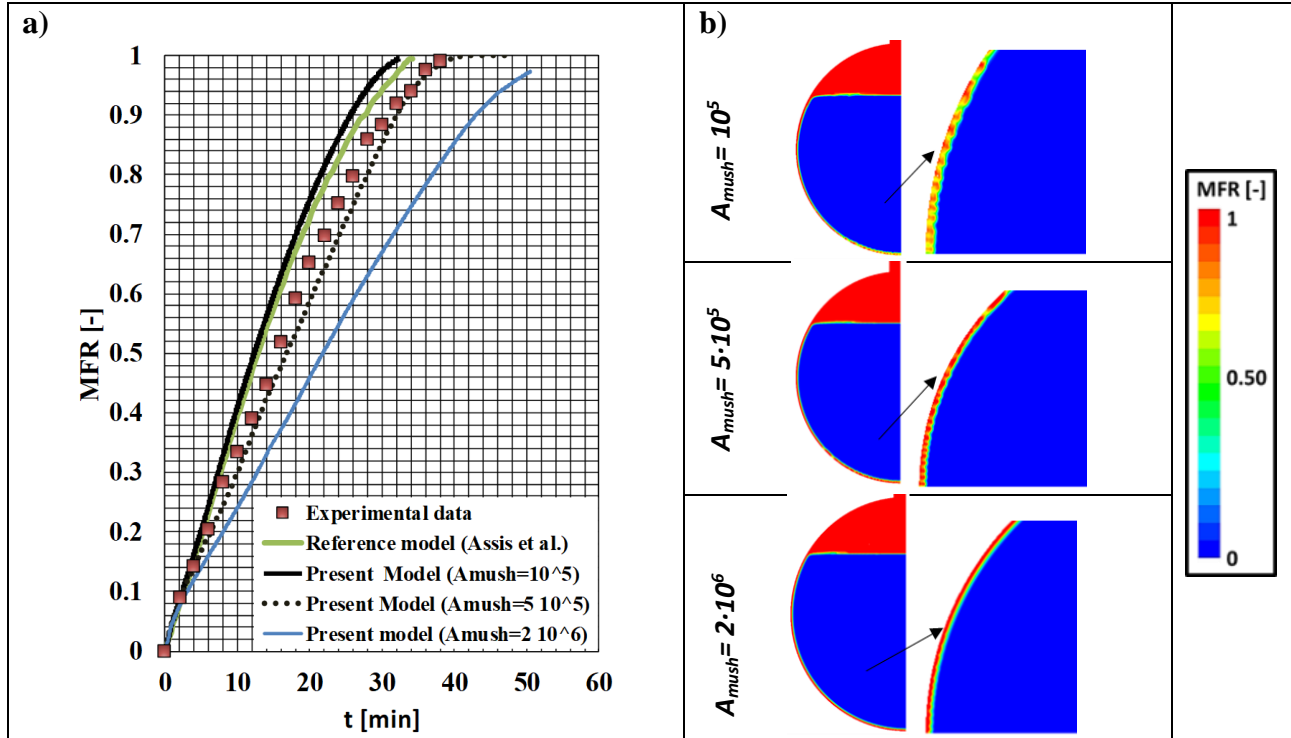

Figure 3. a) Paraffin melt fraction values versus time and b) liquid fraction contours at t= 1 min.

As can be noticed in Figure 3b, visualization of 'structures' resembling to dendrites can be roughly obtained through the dynamically refined grid, with two levels of refinement (the cell size at the area of refinement is almost equal to 200 μm). Since the DAS for $A_{mush=}10^5$ is equal to approximately 1

μm, it is expected that the dendrites representation can be possibly achieved explicitly, if a quite higher local grid resolution is adopted. This is an important outcome, since for the first time it is suggested that the enthalpy porosity approach, coupled with an adaptive local grid method, can potentially reproduce the mushy structure.

Figure 4a. shows numerical results of the PCM melt fraction as a function of time obtained for different values of the A_{mush} parameter. Those results are compared with the ones of Assis et al. model [15]. As can be noticed, numerical results of the current CFD model agree well with the reference paper, as long as high values of the A_{mush} parameter (~10^9) are used. Over and above that, for this case, a limited numerical diffusion is achieved, whilst the melting fraction patterns bear a greater resemblance to the experimental visualizations of Assis et al. [15], than the cases with $A_{mush}=10^5$ and $A_{mush}=10^6$, Figure 4b. Therefore, in order to avoid excess numerical diffusion, during solidification phase, such high values are recommended to be used. It should be stressed out that with such a high value of the A_{mush} the solid phase velocities are set equal to zero artificially and thus, the floating of the solid in the liquid silicon cannot be represented, because the solid PCM does not move. Additionally, in contrast to melting phase, the A_{mush} parameter value does not play such a significant role on the PCM solidification times – since during solidification phase, heat transfer through conduction is the dominant mechanism- but mostly on the induced numerical diffusion.
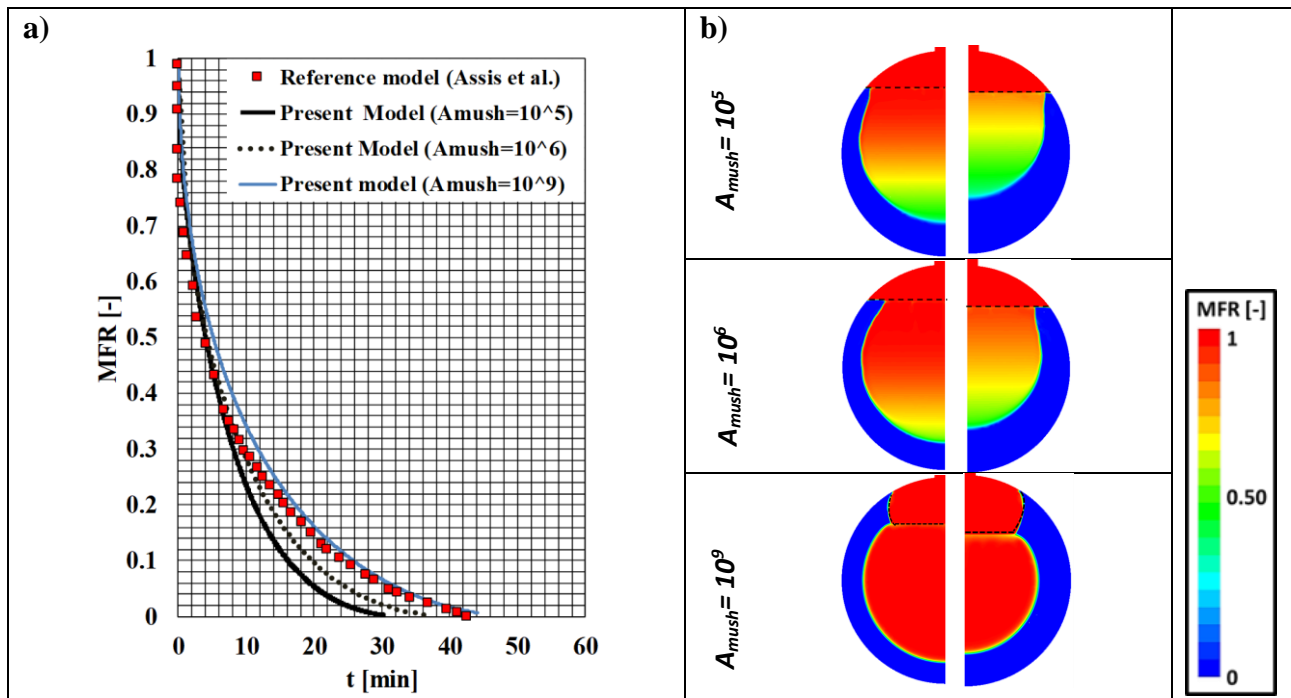

Figure 4. a) Paraffin melt fraction values vs. time and b) liquid fraction contours at t= 5, 10 min.

4.2. Vessel shape investigation

Figure 5 shows contours of silicon liquid fraction for the five geometries tested. As can be noticed, a gradual melting of the PCM occurs from the side to the bottom region at each case. Additionally, the solid material is free to float in the PCM-air interface, thus forcing the liquid silicon aside to a downward movement and in return producing a more rapid melting due to natural convection. This phenomenon observed is the opposite of paraffin wax, which sinks during melting process, whilst its melting is mainly favored in its upper region, due to the molten PCM upward movement.

More specifically, in the beginning of the melting process, the solid silicon is in direct contact with the container walls. During the first seconds of the PCM melting at t=1 min, a thin liquid region of homogeneous shape –a shape similar to that of the heated sidewalls- is formed around the solid phase. This indicates that the dominant mechanism during the initial stages of the melting process is the heat transfer via conduction. Later on, as the liquid region grows more and more over time, natural convection becomes more pronounced, influencing the melting shape of the PCM.
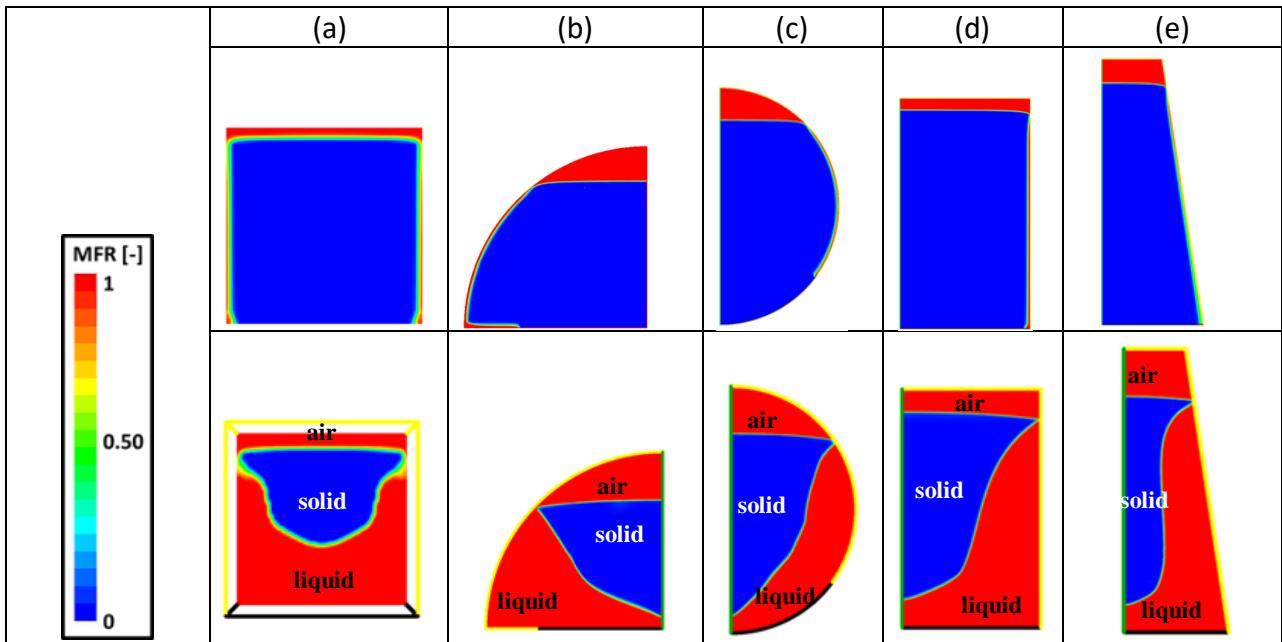
Figure 5. Melt fractions contours at t=1, 20 min for the: a) cube, b) cut-off sphere, c) sphere, d) cylinder, and e) truncated-cone. (Green: axis, yellow: sidewalls and black: emitter).

The quantified evolution of the melting fraction with time for all designs tested is presented in Figure 6a. It can be inferred that the melting process is the slowest in the sphere (~40 minutes) and the fastest in the cube and truncated cone (~ 26-28 min), due to the smaller or larger heated surface, which undermines or enhances the heat transfer process, respectively. Actually, cube and cone are 25 % and 21 % quicker than the sphere, respectively. It is highlighted that even if the cubic shape seems advantageous, it should be noted that during solidification and storage processes the PCM is expected to experience the highest thermal losses, since it has the highest surface area per unit volume.
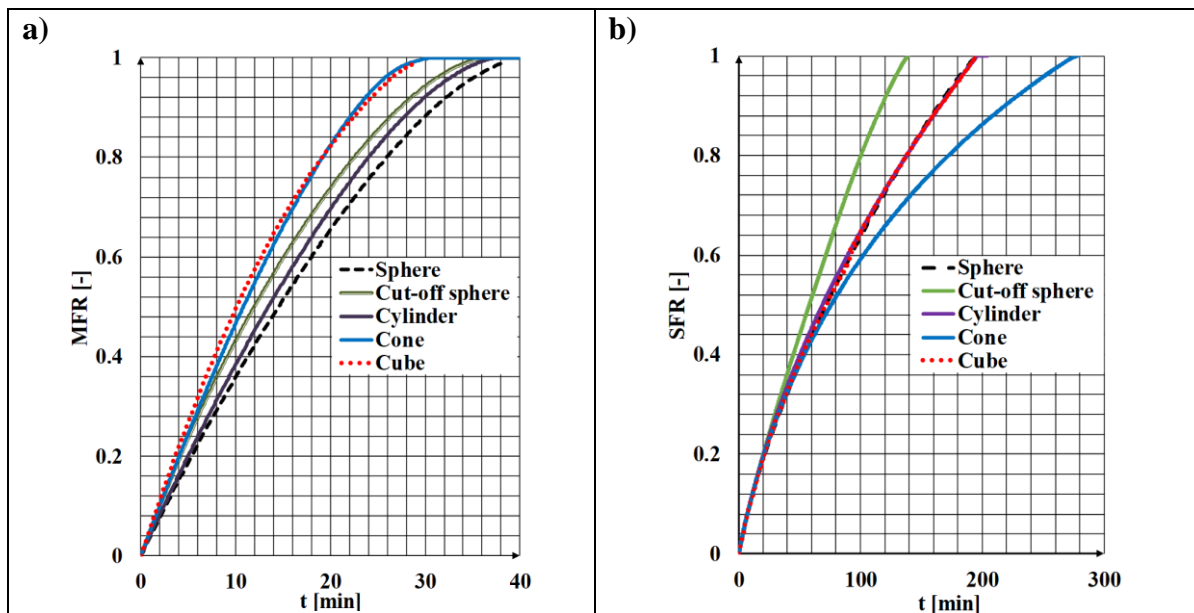

Figure 6. a) Melt and b) solid fraction values versus time for the different geometries tested.

Figure 6b, shows the solidification rates of Si for the five studied geometries. Clearly, the solidification process is the slowest in cone (~280 min) and the fastest in cut-off sphere (~ 140 min), due to its smaller or higher height, Figure 2, which undermines or enhances the heat transfer process, accordingly. The vessel height plays an important role in this problem, since the heat is extracted from the vessel bottom, making the dominant direction of the heat transfer the vessel axis. Actually,

a maximum difference of almost 50% can be observed in the solidification times, between cut-off sphere and truncated-cone –the truncated-cone height is almost two times higher than that of cut-off sphere. In between these two, lie the cube, sphere and cylinder, which almost have the same height.

In this subsection, indicative values of the lateral heat losses during thermal energy storage (TES) period of the studied geometries are also reported. In all cases ambient temperature conditions are considered, whilst insulation of small thermal resistance $\approx$0.002 m^2 K W^{-1} is considered. At t=0 s all geometries are patched with a temperature equal to 2000 ºC. As can be noticed in Table 4, the dominant parameter that affects system heat losses during storage period –for a specific insulation method- is its exterior surface to volume ratio. Therefore, the spherical design, with the lowest surface to volume ratio, is the most favourable in terms of heat losses and is followed by the cylinder and the truncated cone. The cubic design is the worst case, since it has the highest lateral surface to volume ratio, resulting in the highest lateral heat losses, accordingly.

Table 4. Indicative heat losses for the different shapes tested during storage period.

Design	Outer Surface (m^2)	Later heat losses* (kW)	Q_{loss} (kJ)*
Cube	0.135	~ 86.5	~ 5868
Cylinder	0.1248	~ 80	~ 5517
Truncated Cone	0.1296	~ 84	~ 5720
Cut-off sphere	0.1296	~ 85	~ 5756
Sphere	0.1088	~ 73	~ 4891

* At t=60 s after the start of simulation

Taking all into account, the cut-off sphere is the optimum shape among the ones tested, as concerns thermal losses, and charge/discharge rates, Table 5. Apart from this, such a design eliminates the structural tension as it redirects the gravity force or compression forces, downwards in multiple directions. Additionally, its lateral surface, from where heat losses are expected is rather moderate, compared to the rest of the cases tested. The most advantageous, considering stresses and thermal losses, but not so much as regards charge rates, is the sphere. Both geometries would be interesting to construct and test their performance in a compact P2H2P concept; however, the vessel integration in the whole system might be difficult. An alternative option to these and easier and more flexible to construct for such an application is the truncated cone, which also results in high melting rates and moderate heat losses. Its solidification rates even though they are the lowest compared to the rest of the designs tested can be further reduced by altering its tapering ratio (upper to bottom surface ratio).

Table 5. Classification of the different designs tested from the most to the least optimum in terms of a) solidification and b) melting rate and c) heat losses during thermal energy storage period.

	Solidification rate	Melting rate	Minimum Q_{loss} during TES
Selection criteria	Cut-off sphere	Cube	Sphere
	Sphere	Truncated Cone	Cylinder
	Cylinder	Cut-off sphere	Truncated Cone
	Cube	Cylinder	Cut-off sphere
	Truncated Cone	Sphere	Cube

5. Conclusions

This work presents an accurate and efficient computational fluid dynamics (CFD) model, able to describe the transient performance of latent heat thermal energy storage (LHTES) systems operating at ultra-high temperatures (~1410 ºC). Such systems can form part of compact heat-to-electricity devices. The applied methodology combines an adaptive local grid refinement method with the enthalpy porosity approach and the volume of fluid method via proper user defined functions. This model properly considers the effects of a) phase-change material (PCM) volume change, b) buoyancy driven natural convection and c) possible dendrites formation effect on the PCM melting. The model

is validated against numerical and experimental data retrieved from the literature, for paraffin wax solidification/melting at low temperatures (~27 °C). During model validation, the strong effect of the mushy zone parameter, A_{mush}, which is dependent on the PCM structure, on the melting rate has been highlighted. The physical interpretation of this result is that the highest this parameter the smallest the secondary dendrites arm spacing formed inside the PCM and therefore the lowest its melting rate. On top of that, it has been possible to implicitly represent the effect of the dendritic structure formation within the mushy zone, through the dynamically refined grid. During, PCM solidification, a moderate effect of the A_{mush} parameter on the PCM solidification time is traced. However, high values of this parameter should be used to eliminate numerical diffusion.

From a design perspective, one of the key challenges of a LHTES device lies on the identification of the optimum PCM container shape that enables high charging/discharging rates. For this reason, different shapes, i.e. cube, sphere, cut-off sphere, truncated cone and cube, been studied, during silicon solidification/ melting process at ultra-high temperatures. It has been found that the vessel shape plays an important role on the PCM solidification/melting rate. Specifically, the cubic shape results in the highest melting rate, approximately 25 % higher than the one achieved in the sphere. During discharging, the vessel height is a key parameter, since the heat is extracted from the vessel bottom area, making the dominant direction of the heat transfer the vessel axis. Actually, a maximum difference of almost 50% can be observed in the solidification times, between the cut-off sphere and the truncated cone. In summary, the optimum vessel design by taking into account solidification/melting rates, heat losses and expected stresses is the cut-off sphere. However, such a design cannot easily incorporated into a compact P2H2P concept. An alternative and more flexible solution to be constructed is the inversed truncated cone. This design has moderate melting rates and heat losses during thermal energy storage period compared to the rest of geometries tested, but the lowest solidification rate, due to its higher height. Its discharge rates can be further optimized by altering its height. It should be noted that the current model can act as a valuable tool towards the design and optimization of this and similar LHTES systems operating at ultra-high temperatures.

Acknowledgments

Nomenclature

A_{mush}	mushy zone parameter, [-]
Q	heat flux, $W \cdot cm^{-2}$
R	thermal resistance, $m^2 \, K \cdot W^{-1}$
MFR	melt fraction, [-]
SFR	solid fraction, [-]

Subscripts and superscripts

em	emitter
loss	refers to lateral losses, during charge/ discharge and storage period
w	lateral walls

References

[1] Tao YB, He YL. Numerical study on thermal energy storage performance of phase change material under non-steady-state inlet boundary. Applied Energy. 2011;88(11):4172-9.

[2] Datas A, Ramos A, Martí A, del Cañizo C, Luque A. Ultra high temperature latent heat energy storage and thermophotovoltaic energy conversion. Energy. 2016;107:542-9.

[3] Nazir H, Batool M, Bolivar Osorio FJ, Isaza-Ruiz M, Xu X, Vignarooban K, et al. Recent developments in phase change materials for energy storage applications: A review. International Journal of Heat and Mass Transfer. 2019;129:491-523.

[4] Viskanta R. Phase-Change heat transfer. Solar heat storage: Latent heat material, Volume I1983. p. 153-222.

[5] Dhaidan NS, Khodadadi JM. Melting and convection of phase change materials in different shape containers: A review. Renewable and Sustainable Energy Reviews. 2015;43:449-77.

[6] Moore FE, Bayazitoglu Y. Melting Within a Spherical Enclosure. Journal of Heat Transfer. 1982;104(1):19-23.

[7] Lamberg P, Lehtiniemi R, Henell A-M. Numerical and experimental investigation of melting and freezing processes in phase change material storage. International Journal of Thermal Sciences. 2004;43(3):277-87.

[8] Voller VR, Cross M, Markatos NC. An enthalpy method for convection/diffusion phase change. International Journal for Numerical Methods in Engineering. 1987;24(1):271-84.

[9] Tan FL, Hosseinizadeh SF, Khodadadi JM, Fan L. Experimental and computational study of constrained melting of phase change materials (PCM) inside a spherical capsule. International Journal of Heat and Mass Transfer. 2009;52(15):3464-72.

[10] Veeraragavan A, Montgomery L, Datas A. Night time performance of a storage integrated solar thermophotovoltaic (SISTPV) system. Solar Energy. 2014;108:377-89.

[11] Archibold AR, Gonzalez-Aguilar J, Rahman MM, Yogi Goswami D, Romero M, Stefanakos EK. The melting process of storage materials with relatively high phase change temperatures in partially filled spherical shells. Applied Energy. 2014;116:243-52.

[12] Elmozughi AF, Solomon L, Oztekin A, Neti S. Encapsulated phase change material for high temperature thermal energy storage – Heat transfer analysis. International Journal of Heat and Mass Transfer. 2014;78:1135-44.

[13] Pirasaci T, Wickramaratne C, Moloney F, Yogi Goswami D, Stefanakos E. Dynamics of phase change in a vertical PCM capsule in the presence of radiation at high temperatures. Applied Energy. 2017;206:498-506.

[14] Assis E, Katsman L, Ziskind G, Letan R. Numerical and experimental study of melting in a spherical shell. International Journal of Heat and Mass Transfer. 2007;50(9):1790-804.

[15] Assis E, Ziskind G, Letan R. Numerical and Experimental Study of Solidification in a Spherical Shell. Journal of Heat Transfer. 2008;131(2):024502--5.

[16] Fluent, ANSYS FLUENT Release 17.0 User Manual. 2016.

[17] Malgarinos I, Nikolopoulos N, Gavaises M. Coupling a local adaptive grid refinement technique with an interface sharpening scheme for the simulation of two-phase flow and free-surface flows using VOF methodology. Journal of Computational Physics. 2015;300:732-53.

[18] Datas A, Zeneli M, del Cañizo C, Malgarinos I, Nikolopoulos A, Nikolopoulos N, et al. Molten silicon storage of concentrated solar power with integrated thermophotovoltaic energy conversion. AIP Conference Proceedings. 2018;2033(1):090005.

[19] Minakawa S, Samarasekera IV, Weinberg F. Centerline porosity in plate castings. Metallurgical Transactions B. 1985;16(4):823-9.

[20] Gartling DK. Finite element analysis of convective heat transfer problems with change of phase. January 1978.

[21] Hemanth J. Effect of cooling rate on dendrite arm spacing (DAS), eutectic cell count (ECC) and ultimate tensile strength (UTS) of austempered chilled ductile iron. Materials & Design. 1999;21(1):1-8.